HHS Public Access

Author manuscript

Adv Healthc Mater. Author manuscript; available in PMC 2015 July 01.

Published in final edited form as:

Adv Healthc Mater. 2014 July ; 3(7): 1078–1085. doi:10.1002/adhm.201300502.

Track-Etched Magnetic Micropores for Immunomagnetic Isolation of Pathogens

Dr. Melaku Muluneh,

Bioengineering, University of Pennsylvania, 210 South 33rd Street, Suite 240 Skirkanich Hall, Philadelphia, PA 19104-6321, USA

Wu Shang, and

Bioengineering, University of Pennsylvania, 210 South 33rd Street, Suite 240 Skirkanich Hall, Philadelphia, PA 19104-6321, USA

Prof. David Issadore

Bioengineering, University of Pennsylvania, 210 South 33rd Street, Suite 240 Skirkanich Hall, Philadelphia, PA 19104-6321, USA; Electrical and Systems Engineering, University of Pennsylvania, 200 South 33rd Street, 203 Moore Building, Philadelphia, PA 19104-6321, USA

David Issadore: Issadore@seas.upenn.edu

Abstract

A microfluidic chip is developed to selectively isolate magnetically tagged cells from heterogeneous suspensions, the track-etched magnetic micropore (TEMPO) filter. The TEMPO consists of an ion track-etched polycarbonate membrane coated with soft magnetic film ($Ni_{20}Fe_{80}$). In the presence of an applied field, provided by a small external magnet, the filter becomes magnetized and strong magnetic traps are created along the edges of the micropores. In contrast to conventional microfluidics, fluid flows vertically through the porous membrane allowing large flow rates while keeping the capture rate high and the chip compact. By utilizing track-etching instead of conventional semiconductor fabrication, TEMPOs can be fabricated with microscale pores over large areas $A > 1$ cm^2 at little cost (< 5 ¢ cm^{-2}). To demonstrate the utility of this platform, a TEMPO with 5 μm pore size is used to selectively and rapidly isolate immunomagnetically targeted *Escherichia coli* from heterogeneous suspensions, demonstrating enrichment of $\zeta > 500$ at a flow rate of $\Phi = 5$ mL h^{-1}. Furthermore, the large density of micropores ($\rho = 10^6$ cm^{-2}) allows the TEMPO to sort *E. coli* from unprocessed environmental and clinical samples, as the blockage of a few pores does not significantly change the behavior of the device.

1. Introduction

The isolation of biological targets, such as circulating tumor cells (CTCs), pathogenic bacteria, or circulating microvesicles (CμVs) from easily accessible biological fluids is of great importance for disease monitoring and diagnostics.[1–4] Detection platforms that utilize micro- and nanoscale structures, where dimensions can be designed to match those of the

Correspondence to: David Issadore, Issadore@seas.upenn.edu.

targeted object, have been utilized for highly selective sorting.[2,4–6] One modality that has been particularly successful for isolating cells from clinical samples is magnetophoresis, in which immunomagnetically labeled targets are isolated from suspensions using strong and highly localized magnetic forces.[7–9] Due to the inherently negligible magnetic susceptibility of biological material, magnetically labeled cells can be sorted directly from unprocessed clinical (e.g., blood)[10] and environmental (e.g., drinking water)[11] samples. Furthermore, strong forces can be applied without the need for a power supply or moving parts, making magnetic sorting well suited for use in practical settings outside of the laboratory.[12]

Much work has been done to develop and improve magnetic isolation using microfabrication techniques.[13–20] Micropatterned magnetic field profiles have been engineered using lithographically defined current carrying wires and magnetic materials.[13,14,19–22] Additionally, a number of bottom-up fabrication strategies have been developed to create strong magnetic forces without lithography.[15,18] In conjunction with patterned magnetic fields, microfluidic channels have been used to deliver cells to the regions of high magnetic field gradients, to provide predictable flow velocities, and to minimize nonmagnetic retention.[9,13,17,19,20,22] However, the limited throughput and susceptibility to clogging of microscale devices, make these approaches unsuitable for many practical applications.

Here, we report the development of a new approach to magnetic separation that achieves high sorting enrichment and throughput, can sort cells from unprocessed samples, and which can be implemented on a chip that costs little to manufacture. The track-etched magnetic micropore (TEMPO) filter consists of an ion track-etched polycarbonate membrane coated with a soft magnetic film, permalloy ($Ni_{20}Fe_{80}$). In contrast to conventional microfluidic devices, fluid flows vertically through the porous membrane allowing large flow rates, while keeping the capture rate high, and the chip compact. We replace the semiconductor processing used in previous studies,[14] with commercially available ion track-etched polycarbonate membranes. Unlike semiconductor processing, polycarbonate membranes can be fabricated with microscale pore sizes, over large areas ($A > 10$ cm^2), for little cost (<5 ¢ cm^{-2}) (Whatman). The strong magnetic forces and large cross-sectional area of the TEMPO filter enable highly efficient cell separation, enriching magnetic species from nonmagnetic ones by a factor of $\zeta > 10^4$ at high flow rates ($\Phi > 10$ mL h^{-1}). Furthermore, the large density of micropores ($\rho = 10^6$ pores cm^{-2}) reduces the risk of clogging from clinical and environmental samples, as the blockage of a few pores does not significantly change the behavior of the device. To demonstrate the utility of this platform, a chip with a 5 μm pore size TEMPO was used to isolate immunomagnetically labeled *Escherichia coli* from a suspension of similarly sized bacteria spiked into unprocessed clinical and environmental samples.

2. Experimental Design

The TEMPO filter consists of a track-etched polycarbonate membrane coated with a thin layer of soft magnetic material (Figure 1a). The micropores create large gradients ∇B (Figure 2a), which imparts strong magnetic forces $F \sim (B \cdot \nabla)B$ on magnetic nanoparticle

(MNP)-labeled cells as they pass through the pores. Targeted cells are trapped and isolated from the unlabeled cells, which flow through the filter unimpeded. The chip sits in a large uniform magnetic field $|B| = 0.2$ T provided by a small external NdFeB magnet. The external magnet is an axially magnetized cylinder with a 1.5″ diameter and 0.5″ thickness and a surface field of 4105 Gauss (K & J Magnetics, DX88-N52). This field magnetizes both the MNP-labeled cells and the soft magnetic material on the TEMPO filter. When the NdFeB magnet is removed, the force disappears and the trapped cells can be released.

The basic physical principle of capturing cells on a TEMPO can be broken into two steps. First, as a cell approaches a micropore it experiences a magnetic force F_m that pulls it towards the edge of the pore. The magnetic field gradient is maximized at the pore's edge, creating a trap. If the magnetic trapping force F_m is larger than the drag force F_d, the cell will remain in the trap. The fraction of magnetically targeted cells that are successfully captured by the TEMPO chip is the product of the fraction that are brought to the edge of the pore and the fraction that are successfully trapped once brought there.

There are three main elements of the TEMPO, which maximize the magnetic force F_m and minimize the drag force F_d on targeted cells, and thus optimize its ability to capture magnetically labeled cells.

1. Strong magnetic field with high field gradient ($B\uparrow$, $\nabla B\uparrow$). The magnetic force $F_m \sim (B\nabla)\, B$ is maximized by increasing the strength of the applied field B and its spatial changes ∇B. The TEMPO filter generates large fields ($|B| \approx 0.2$ T) due to the external NdFeB magnet and strong, highly localized magnetic field gradients due to the micropore geometry (Figure 2).
2. Large flow channel area ($\nu\downarrow$). The hydrodynamic drag force $F_d \propto \nu$ is minimized by decreasing the flow velocity ν for a given flow rate $\boldsymbol{\Phi}$. The flow velocity is inversely proportional to the cross-sectional area of the flow channel $\nu \propto 1/A$ The cross-sectional area of the TEMPO grows quadratically with the dimensions of the chip $A \propto L^2$, rather than linearly as with lateral flow, thus enabling vertical flow devices to achieve high flow rates on compact chips. The flow velocity is distributed across the micropores and is kept small by the large pore density ($\rho = 10^6$ pores cm^{-2}) of the track-etched membranes.
3. Close proximity of each cell to the regions of strong magnetic force ($r\downarrow$). Because each cell must pass through a micropore, each cell comes within $r = d/2$ of the edge of the pore, where d is the micropore diameter. By choosing the pore size to be on the same size-scale as the object being trapped, it can be ensured that each cell comes within close proximity of the high-force trapping region.

2.1. Device Fabrication

To demonstrate the technique of using a TEMPO to sort cells, we fabricated a prototype filter with a $d = 5$ μm pore size. We coated a polycarbonate track-etched film (Whatman, Nuclepore) with permalloy (200 nm, $Ni_{20}Fe_{80}$) and a passivation layer (30 nm, Au) using thermal evaporation (Kurt Lesker PVD-75, Wolf NanoFab, University of Pennsylvania). Figure 1d shows a scanning electron micrograph (JEOL 7500F HRSEM, The Laboratory for

Research on the Structure of Matter, University of Pennsylvania) of a 5 μm diameter micropore TEMPO, with the gold, permalloy, and polycarbonate layer visible.

The TEMPO was integrated into a laser-cut laminate sheet microfluidic chip (Figure 1c). On this chip, a "shower head" geometry was used (Figure 1c) to evenly distribute fluid to the TEMPO to optimize sorting enrichment. Symmetric branching was used to split the flow evenly to sixteen 0.5 mm^2 holes above the TEMPO. Figure 1d shows a stereoscope image of the "shower head." Underneath the TEMPO is a thick (200 μm) channel that brings the fluid to the output. The microfluidic channel patterns were defined using laser-cutting (VLS3, VersaLaser). The base was constructed using 1.5 mm thick extruded poly(methyl methacrylate) sheet (McMaster Carr). The device was connected to a syringe pump using blunt syringe tips (McMaster Carr) epoxied onto the top layer of the microfluidic chip. The device was pretreated with Pluronic F-127 (Sigma–Aldrich) to minimize non-specific retention of cells to the channel walls or to the TEMPO.

2.2. Immunomagnetic Labeling of Bacteria

To evaluate the capability of the TEMPO filter for cell sorting, we performed a negative enrichment of *E. coli* suspended among a population of *Staphylococcus aureus*. Fresh *E. coli* bacteria samples (Invitrogen) were grown overnight in Luria-Bertani (LB) broth at 37 °C in 14 mL round-bottom tubes with rotary shaking for about 6 h. The concentrations of the *E. coli* bacteria stock solutions were quantified using a Varian Cary 100 Bio UV–vis Spectrophotometer. *S. aureus* prelabeled with Alexa Fluor 594 were used (*Staphylococcus aureus* BioParticles, Life Technologies).

An indirect labeling method was utilized to magnetically label the *E. coli*, in which the bacteria were first targeted with biotinylated antibody and subsequently tagged with anti-biotin MNPs. Biotinylated anti-*E. coli* polyclonal antibody (80 μL, 3.2 mg mL^{-4}; Thermo Scientific) and the diluted *E. coli* bacterial sample (80 μL, 1×10^7–9×10^7 cell mL^{-1}) were mixed and incubated at room temperature for 1 h. Subsequently, the sample was washed twice. Anti-biotin superparamagnetic nanoparticles, 50 nm in diameter, (20 μL, Miltenyi Biotec) were added and incubated at 4 °C for 15 min.[23] The sample was subsequently centrifuged and resuspended. The nanoparticle conjugated bacteria sample and a control were measured by a Burker Minispec MQ60 NMR analyzer to quantify labeling, which showed that there were 2300 particles per cell. For fluourescence detection, SYTO9 stain (500 mL, 10×10^{-6} M, Life Technologies) was added into the nanoparticle conjugated bacteria sample and 15 min room temperature incubation was allowed. The sample was then washed three times with phosphate buffer saline (PBS) to remove residual stain.

To demonstrate background insensitivity, the prepared *E. coli* and *S. aureus* samples were spiked into 800 μL of multiple samples (PBS, PBS with excess MNPs (10^8/mL), oral lavage from a healthy volunteer, and local river water). The oral lavage was collected by having a healthy volunteer rinse his mouth for 30 s with sterile saline solution. The river water was collected from the Schuylkill river in Philadelphia, PA.

2.3. Characterization

2.3.1. Finite Element Simulations—Finite element magnetic field simulations (Maxwell, Ansoft) were used to aid the design and characterization of the TEMPO filter. The simulated magnetic field strength B was plotted on the cross-section of the self-assembled magnetic filter (Figure 2a). The magnetic field strength drops rapidly in distance from the surface of the magnetic layer, to create large gradients that lead to strong magnetic forces. The TEMPO was modeled as an axially symmetric membrane with a 5-μm diameter pore, coated with 200 nm of permalloy $Ni_{20}Fe_{80}$ (Maxwell, Ansoft). To polarize the nanoparticles and the permalloy film, a NdFeB magnet was included 0.5 cm below the TEMPO filter with a 1.5″ diameter, 0.5″ thickness, and a surface field of 4105 Gauss. The boundary conditions were set such that the magnetic field was zero at large distances (d > 10″) from the magnet.

The magnetophoretic force F_m on a magnetic bead as it passes through a micropore was calculated by combining the finite element simulation from Figure 2a with a simplified model for the bead.[24–26] The calculated force is localized within ≈2 μm of the pore's edge (Figure 2b). The ability of the pore to capture passing cells is therefore optimized when the pore diameter is small enough to bring the cells in close proximity to the edge. The model assumes a d = 1 μm magnetic bead that is fully magnetized by the applied |B| ≈ 0.2 T field, with a saturation magnetization m_s= 1.7 mA μm^2. This value was extrapolated from previous measurements using superconducting quantum interference device magnetometry.[25] The magnetic force F_m was calculated by combining this magnetic moment **m** with the simulated magnetic field $\boldsymbol{B}$, $\boldsymbol{F}_m = (\mathbf{m}\cdot\nabla)\mathbf{B}$. These results can be extended to calculations of the force on a magnetically labeled cell. The magnetic moment of the cell is directly proportional to the number of nanoparticles bound to the cell n and the magnetic moment m_p of the particle ($m = n * m_p$).[27,28]

Once an object is brought to the edge of the pore, the competition of the magnetic force (Figure 2c) and the drag force from the passing fluid determine whether the object gets trapped. The drag force is given by Stokes' law $F_d = 6\pi\eta r v$, where η = 0.8 mPa*s is the viscosity of water and r = 0.5 μm is the diameter of the bead. The average velocity can be calculated through the pores $v_{avg} = \Phi/(\rho A_p A)$ where $\rho = 10^6$ pores cm^{-2} is the pore density, (Whatman) A_p is the cross-sectional area of an individual pore, and A = 0.39 cm^2 is the cross-sectional area of the membrane. The flow profile through a single pore $v \propto (1-(r/a)^2)^{1/2}$ can be calculated based on the Stokes' equations of motion.[29] The flow velocity is greatest in the center of the pore, and therefore the drag force F_d is minimal at the edges of the pore where the trap is located. Using this model, once trapped a 1-μm magnetic bead will remain trapped at flow rates Φ > 100 mL h^{-1}. We therefore conclude that the flow rate limit of the device does not arise from the competition of trapped beads and the drag force, and instead comes from the fraction of beads that come into contact with the magnetic traps. By increasing the number of opportunities for a cell to pass in close proximity to the edge of a pore, the enrichment rate could therefore be enhanced. We hypothesized that this enhancement could be realized by adding additional TEMPOs in series.

2.3.2. Experimental Characterization—The TEMPO filter was first tested by sorting magnetic from nonmagnetic polystyrene beads. A suspension that contained both 1 μm diameter fluorescent polystyrene beads (FluoSpheres Polystyrene Microspheres, 1.0 μm; Invitrogen) and 1 μm diameter fluorescent magnetic beads (Spherotech) was pumped through the TEMPO. The input (Figure 3a) and output (Figure 3b) were measured using flow cytometry (LSR II, BD), and the enrichment of the TEMPO was analyzed. Because we characterized the ability of the filter to selectively capture magnetic beads by counting the magnetic beads that the filter did not capture relative to nonmagnetic beads, we used higher concentrations of magnetic than nonmagnetic beads. For each test, we used 1 mL of a suspension that included 1×10^6 magnetic beads and 5×10^4 nonmagnetic beads. The three parameters of the magnetic sorting device that we characterized were enrichment $\zeta = (C_{1p}/C_{1m})/(C_{0p}/C_{0m})$, purity C_{om}/C_{0p}, and flow rate $\boldsymbol{\Phi}$, where C_{0p} and C_{1p} are the concentration of non-targeted cells before and after sorting, respectively, and C_{0m} and C_{1m} are the concentration of targeted cells before and after sorting, respectively.

To validate the basic operating principal of the TEMPO, we first compared the performance of the TEMPO to two control devices, one which lacked the permalloy coating on its polycarbonate membrane and one for which the external magnet was removed (Figure 3c). The TEMPO device, with an external magnet in place and with a permalloy coating, demonstrated highly enriching sorting ($\zeta = 7300$ at $\boldsymbol{\Phi} = 3$ mL h^{-1}). When the external magnet was removed, and the superparamagnetic beads and the permalloy film were no longer magnetized, the enrichment ceased ($\zeta \approx 1$). A slight enrichment was observed when the external magnet was in place but the permalloy coating was not ($\zeta = 1.5$). However, the enhancement in the enrichment ζ due to the addition of the permalloy coating, and the strong magnetic field gradients ∇B that it creates, was 5000× compared with the enrichment from just the external magnet.

The TEMPO demonstrated highly enriching sorting at flow rates as great as 60 mL h^{-1} (Figure 3d). The enrichment was observed to be a function of flow rate, following a power law dependency, $\boldsymbol{\Phi} \propto \zeta^m$ where $m = -3.74$ ($R^2 = 99.9\%$) over several orders of magnitude (Figure 3e). By increasing the area of the filter from $A_o = 0.6 \times 0.6$ cm^2 to an area $A = 4A_o$, the enrichment curve shifted to the right proportionally. By increasing the area of the TEMPO, the flow rate was distributed over a proportionately greater number of micropores, decreasing the average flow velocity through each pore and therefore increasing the enrichment. The linear shift in the flow rate with increasing area A supports the hypothesis that the flow was distributed uniformly. The power-law dependency m was invariant to changes in filter size A, suggesting that the power law dependency comes from an intrinsic property of the micropore and sample geometry. The linear scaling of the flow rate $\boldsymbol{\Phi}$ with the area A of the filter allows chips to be designed with a large range of flow rates appropriate for specific applications.

Based on our finite element simulations, we hypothesized that enrichment could be improved by placing several TEMPO filters in series. The TEMPO filters were stacked vertically, using a slight modification to the fabrication strategy for the single filter devices. One layer of 200 μm thick laser cut mylar was placed between each TEMPO filter.

Additional flow splitters were not necessary for each layer, as the flow remained evenly distributed as it passed through the vertically integrated filters.

There was an exponential increase observed in sorting enrichment for each addition layer of TEMPO (Figure 4a). The exponential increase is understood by assuming that each filter enriches its input by an amount ζ_0, independent of any of the other filters. If each subsequent filter receives the previous filter's output as its input, then the enrichment after n stages is $\zeta = (\zeta_0)^n$. To test this effect, we measured the enrichment ζ of four different chips, with n = 1, 2, 3, and 4 filters (Figure 4b). The enrichment ζ fits well to an exponential $\zeta \propto e^{bn}$, with b = 1.84 (R^2 = 99.8%). This exponential growth allows for large improvements in enrichment to made by adding additional filters. For instance, by increasing from n = 1 to n = 4 for an A = 0.36 cm^2 TEMPO at $\boldsymbol{\Phi}$ = 10 mL h^{-1}, enrichment was improved 250×.

Release of cells is important for applications where downstream analysis is desired on whole cells, such as immunostaining,[6] single cell genotyping,[30] or micro-Hall magnetometry.[27,28] The TEMPO filter has the advantage that when the external magnet is removed, the magnetic force disappears, and the trapped cells can be released. This feature is facilitated by the low magnetic remanence of permalloy $Ni_{20}Fe_{80}$, which brings the magnetization to zero when the external magnet is taken away. The trap and release protocol is outlined in Figure 5. First, the targeted cells are trapped and concentrated by passing the sample through the TEMPO filter with the external magnet in place (Figure 5a). Next, cells and debris that were not trapped are washed away by passing buffer solution through the TEMPO (Figure 5b). Finally, the external magnet is removed and the trapped cells are released into the passing buffer solution (Figure 5c). To demonstrate this functionality, we trapped magnetic beads from a suspension of non-magnetic beads, washed, and then subsequently released them (Figure 5d). The image was taken using an epi-fluorescence microscope with a 10× air objective (Leica, DM4000B) looking down onto the TEMPO filter. We quantitatively measured the purity of the output of the released beads, which is >95% and did not significantly change with additional layers of TEMPO (P > 0.5, a two-tailed t-test) (Figure 5e).

The ability of the TEMPO filter to sort bacteria was demonstrated by negatively enriching *E. coli* bacteria that were tagged with anti-*E. coli* MNPs (Figure 6a). Prior work has demonstrated sorting of *E. coli* using immunomagnetic labeling and microfluidic chips.[17,31] However, the use of conventional microfluidic sorting structures has limited throughput and has made these approaches susceptible to clogging.

We first characterized the TEMPO's capability of sorting the *E. coli* from a suspension of *S. aureus*. We utilized a TEMPO with n = 3 filters, an area A = 0.8 cm^2, and a pore size of d = 5 μm. Both the *S. aureus* (0.6 μm diameter) and *E. coli* (2 μm long and 0.25–1 μm in diameter) have sizes smaller than the pore size of the filter, ensuring that they would not be trapped based on size. The change in the composition of the suspension before and after filtration was measured by flow cytometry. The input (Figure 6b) and output (Figure 6c) were measured, and the sorting enrichment of the TEMPO was analyzed. Because the TEMPO captured *E. coli* very effectively (ζ= 600), we introduced many more *E. coli* than *S.*

aureus to the TEMPO to measure the rare *E. coli* that the TEMPO missed. For each test, we used a 1-mL suspension that included 9.2×10^5 *E. coli* and 9×10^4 *S. aureus*.

At a flow rate of $\Phi = 5$ mL h^{-1}, enrichment of $\zeta = 600$ was achieved. Enrichment was measured at flow rates up to $\Phi = 40$ mL h^{-1} (Figure 6d). The sorting enrichment was observed to drop predictably as a function of flow rate, following a power law dependency, $\Phi \propto \zeta^m$ where $m = -1.524$ ($R^2 = 93.8\%$) over several orders of magnitude. Greater enrichment ζ at higher flow rates Φ could be obtained by enlarging the area of the filter A ($\Phi = A\Phi_0$) or the number of filters n($\zeta = \zeta_0^n$), as was shown in the sections above.

The enriched population of *E. coli* could be imaged in realtime as they were trapped onto the TEMPO using fluorescence microscopy (Figure 6e). The TEMPO device was run under an epifluorescence microscope with a 10× air objective (Leica, DM4000B) looking down onto the filter. Because individual bacteria could be imaged on the TEMPO and because of the high capture rate of the TEMPO (ζ= 600), the theoretical limit of detection is that of a single bacteria. Alternatively, the TEMPO can be used to negatively select off-target bacteria and the targeted cells can be concentrated and imaged downstream using size-based capture.[32]

The TEMPO's insensitivity to background and clogging was tested by enriching *E. coli* across various media. We compared measurements of enrichment in buffer with measurements in three examples of practical samples: a clinical sample, an environmental sample, and a sample with an excess of MNPs to demonstrate wash-free use. For each test, we spiked a 1-mL sample with 8×10^5 *E. coli* and 6×10^4 *S. aureus*.

First, we tested oral lavage obtained from a healthy volunteer (Figure 6f). Oral lavage is commonly used for the diagnosis of oral infections, and samples include a heterogeneous suspension of bacteria including *A. actinomycetemcomitans* (Aa), *P. gingivalis* (Pg), *T. forsythensis* (Tf), *P. intermedia* (Pi), and *M. micros*(Mm).[33] The observed enrichment ζ from oral lavage and in PBS was statistically identical ($P > 0.5$, a two-tailed t-test), verifying that the complex background of the clinical samples had a negligible effect on TEMPO sorting. Further comparisons were made on samples with excess MNPs (10^8 particles mL^{-1}) and on an environmental sample collected from the Schuylkill river in Philadelphia[34] (Figure 6f). In both cases, the measured enrichment was found to be statistically identical ($P > 0.5$, a two-tailed t-test) to that measured in PBS.

Both the clinical and environmental sample contained particulates larger than the pore size of the TEMPO ($d = 5$ μm);[33,34] however due to the large density of micropores ($\rho = 10^6$ cm^{-2}), the blockage of a few pores did not significantly change the behavior of the device. Additionally, due to the use of magnetic sorting, the MNP-labeled cell could be sorted directly from the unprocessed clinical and environmental sample without interference from salinity, turbidity, or PH.

3. Conclusions

We have developed a novel technology for isolating biological targets, the TEMPO filter. The TEMPO filter uses the following elements to maximize sorting selectivity at very high flow rates. 1) Strong magnetic field B and gradients ∇B, to create strong magnetic traps, 2)

A large area flow channel to obtain low hydrodynamic drag forces F_d at high flow rates Φ, and 3) Close proximity for each cell to the region of strong magnetic forces via its micropore geometry. With such properties, the filter can efficiently isolate and trap cells ($\zeta > 10^4$) at very high flow rates ($\Phi > 10$ mL h^{-1}). Furthermore, the TEMPO was demonstrated capable of selectively sorting bacteria from practical environmental and clinical samples without extensive sample processing or purification. The TEMPO filter offers advantages for a wide range of biomedical applications, beyond the isolation of bacteria that was demonstrated in this paper. Track-etching allows the pores of the TEMPO filters to be scaled from 100 μm down to 30 nm, for optimal trapping of objects as small as 50 nm exosomes and as large as 15 μm CTCs.

Further development of the TEMPO filter for increased flow rate and improved manufacturability is possible. The thermal evaporation of magnetic material could be replaced with techniques more suitable for large-scale manufacturing such as sputtering or electroplating.[35] Flow rate can be further improved by enlarging the cross-sectional area A of the filters. Extrapolating from the results of this paper, an $A = 100$ cm^2 device could efficiently enrich a sample at a flow rate of $\Phi = 3$ L h^{-1}. At such flow rates, the TEMPO could be applied to the isolation of contaminants in samples with very large volumes, such as industrial or agricultural runoff.

Acknowledgments

The authors gratefully thank the staff of the Wolf Nanofabrication Facility for advice during device fabrication and undergraduate researchers Kinjal Shah, Julia D'Souza, and Nishant Neel for their assistance with simulations and bacteria processing. This work is supported by the Department of Bioengineering, University of Pennsylvania, a pilot grant from the University of Pennsylvania Nano/Bio Interface Center, National Science Foundation DMR 08-32802, and a pilot grant from the University of Pennsylvania Center for AIDS Research (AI 045008).

References

1. Fan R, Vermesh O, Srivastava A, Yen BKH, Qin L, Ahmad H, Kwong GA, Liu CC, Gould J, Hood L, Heath JR. Nat Biotechnol. 2008; 26:1373. [PubMed: 19029914]
2. Ferguson BS, Buchsbaum SF, Wu TT, Hsieh K, Xiao Y, Sun R, Soh HT. J Am Chem Soc. 2011; 133:9129. [PubMed: 21561070]
3. Chen GD, Alberts CJ, Rodriguez W, Toner M. Anal Chem. 2009; 82:723. [PubMed: 19954210]
4. Chen C, Skog J, Hsu CH, Lessard RT, Balaj L, Wurdinger T, Carter BS, Breakefield XO, Toner M, Irimia D. Lab Chip. 2010; 10:505. [PubMed: 20126692]
5. Chen J, Li J, Sun Y. Lab Chip. 2012; 12:1753. [PubMed: 22437479]
6. Nagrath S, Sequist LV, Maheswaran S, Bell DW, Irimia D, Ulkus L, Smith MR, Kwak EL, Digumarthy S, Muzikansky A, Ryan P, Balis UJ, Tompkins RG, Haber DA, Toner M. Nature. 2007; 450:1235. [PubMed: 18097410]
7. Zborowski, M.; Chalmers, JJ. Magnetic Cell Separation. Elsevier; Amsterdam: 2011.
8. Miltenyi S, Müller W, Weichel W, Radbruch A. Cytometry. 1990; 11:231. [PubMed: 1690625]
9. Pamme N. Lab Chip. 2006; 6:24. [PubMed: 16372066]
10. Ozkumur E, Shah AM, Ciciliano JC, Emmink BL, Miyamoto DT, Brachtel E, Yu M, Chen Pi, Morgan B, Trautwein J, Kimura A, Sengupta S, Stott SL, Karabacak NM, Barber TA, Walsh JR, Smith K, Spuhler PS, Sullivan JP, Lee RJ, Ting DT, Luo X, Shaw AT, Bardia A, Sequist LV, Louis DN, Maheswaran S, Kapur R, Haber DA, Tonerothers M. Sci Transl Med. 2013; 5:179ra47.
11. Ramadan Q, Gijs MAM. Microfluid Nanofluid. 2012; 13:529.

12. Issadore, D.; Westervelt, R. Point-of-Care Diagnostics on a Chip. Springer; Heidelberg, Germany: 2012.
13. Adams JD, Kim U, Soh HT. Proc Natl Acad Sci USA. 2008; 105:18165. [PubMed: 19015523]
14. Earhart CM, Wilson RJ, White RL, Pourmand N, Wang SX. J Magn Magn Mater. 2009; 321:1436. [PubMed: 20161248]
15. Issadore D, Shao H, Chung J, Newton A, Pittet M, Weissleder R, Lee H. Lab Chip. 2011; 11:147. [PubMed: 20949198]
16. Pamme N, Wilhelm C. Lab Chip. 2006; 6:974. [PubMed: 16874365]
17. Xia N, Hunt TP, Mayers BT, Alsberg E. Biomed Microdevices. 2006; 8:299. [PubMed: 17003962]
18. Nawarathna D, Norouzi N, McLane J, Sharma H, Sharac N, Grant T, Chen A, Strayer S, Ragan R, Khine M. Appl Phys Lett. 2013; 102:063504.
19. Plouffe BD, Mahalanabis M, Lewis LH, Klapperich CM, Murthy SK. Anal Chem. 2012; 84:1336. [PubMed: 22240089]
20. Lee H, Jung J, Han SI, Han KH. Lab Chip. 2010; 10:2764. [PubMed: 20820486]
21. Lee H, Liu Y, Westervelt RM, Ham D. Solid-State Circuits IEEE J. 2006; 41:1471.
22. Kim S, Han SI, Park MJ, Jeon CW, Joo YD, Choi IH, Han KH. Anal Chem. 2013; 85:2779. [PubMed: 23384087]
23. Zhang H, Moore LR, Zborowski M, Williams PS, Margel S, Chalmers JJ. Analyst. 2005; 130:514. [PubMed: 15776162]
24. Furlani EP, Ng KC. Phys Rev E. 2006; 73:061919.
25. Shevkoplyas SS, Siegel AC, Westervelt RM, Prentiss MG, Whitesides GM. Lab Chip. 2007; 7:1294. [PubMed: 17896013]
26. Forbes TP, Forry SP. Lab Chip. 2012; 12:1471. [PubMed: 22395226]
27. Issadore D, Chung J, Shao H, Liong M, Ghazani AA, Castro CM, Weissleder R, Lee H. Sci Transl Med. 2012; 4:141ra92.
28. Issadore D, Chung HJ, Chung J, Budin G, Weissleder R, Lee H. Adv Healthcare Mater. 2013; 2:1224.
29. Hasimoto H. J Phys Soc Japan. 1958; 13:633.
30. Zeng Y, Novak R, Shuga J, Smith MT, Mathies RA. Anal Chem. 2010; 82:3183. [PubMed: 20192178]
31. Lee JJ, Jeong KJ, Hashimoto M, Kwon AH, Rwei A, Shankarappa SA, Tsui JH, Kohane DS. Nano Lett. 2014; 14:1. [PubMed: 23367876]
32. Chung J, Issadore D, Ullal A, Lee K, Weissleder R, Lee H. Biomicrofluidics. 2013; 7:054107.
33. Boutaga K, Savelkoul PHM, Winkel EG, van W, Arie J. J Periodontol. 2007; 78:79. [PubMed: 17199543]
34. Interlandi SJ, Crockett CS. Water Res. 2003; 37:1737. [PubMed: 12697218]
35. Smistrup K, Lund-Olesen T, Hansen MF, Tang PT. J Appl Phys. 2006; 99:08P102.

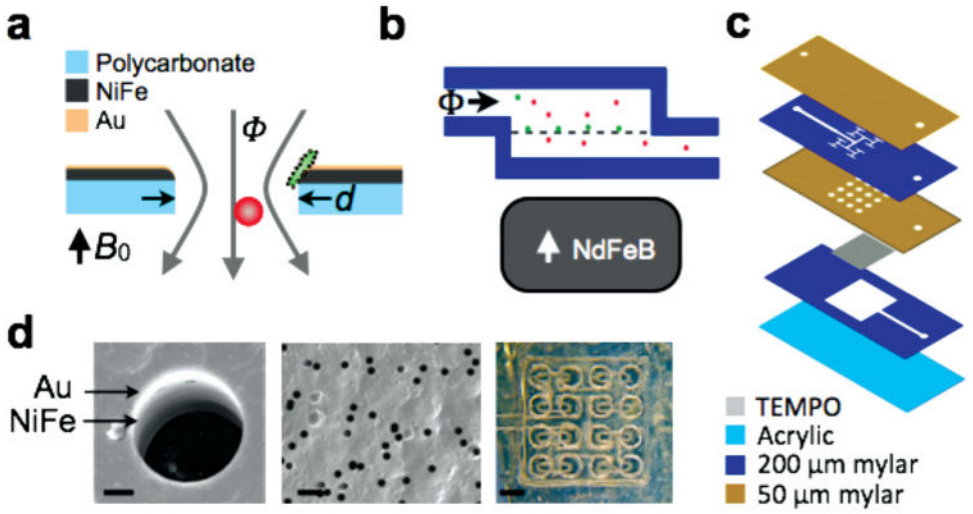

Figure 1.

The track-etched magnetic micropore (TEMPO). a) A schematic of a single TEMPO micropore with diameter *d* coated with permalloy ($Ni_{20}Fe_{80}$) and a passivation layer of gold (Au). Cells flow vertically with flow rate **Φ** through the pore. In an applied field B_o, the TEMPO and the magnetically labeled cells are magnetized. The magnetically labeled cells (green) are trapped and unlabeled cells (red) pass through unabated. b) A cross-section of the microfluidic chip, showing the external NdFeB permanent magnet. c) An exploded view of the laminate sheet microfluidics. d) SEM images of a TEMPO filter, with the Au and NiFe layer visible. The far right figure is a stereoscope image of the “shower head” microfluidics. The scale bars (from left to right) are 2, 25, and 800 µm.

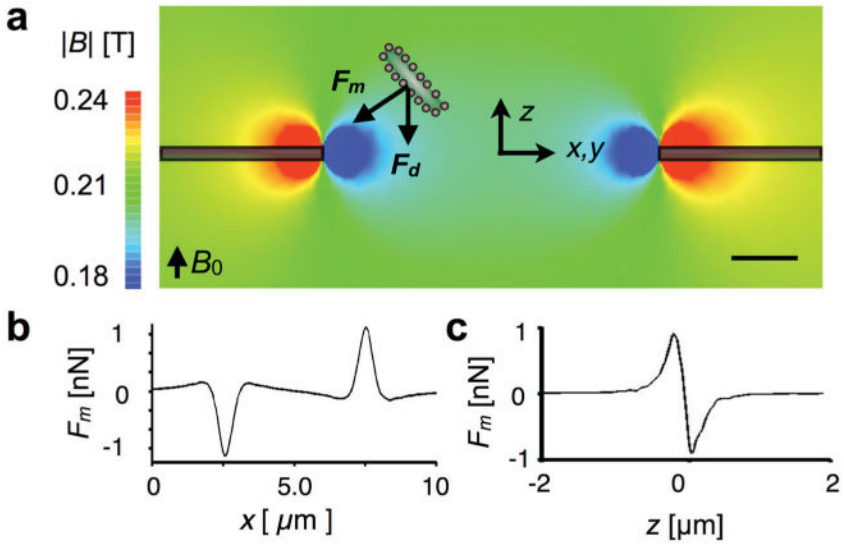

Figure 2.

Characterizing the TEMPO with finite element simulations. a) Magnetic field simulations. The magnetic field strength |B| is plotted on the cross-section of an individual d = 5 μm micropore. A magnetically labeled cell is pulled towards the edge of the TEMPO with a magnetic force F_m. To trap the cell, the magnetic force F_m must overcome the drag force F_d. The scale bar is 1 μm. b) The magnetic force on a 1 μm diameter magnetic microbead is plotted as a function of x, Δz = 500 nm above the TEMPO. The force is localized laterally within ≈2 μm of the pore's edge. c) The magnetic trapping force is plotted vs z Δx = 500 nm from the edge of the micropore. The force is localized vertically within ≈ 1 μm.

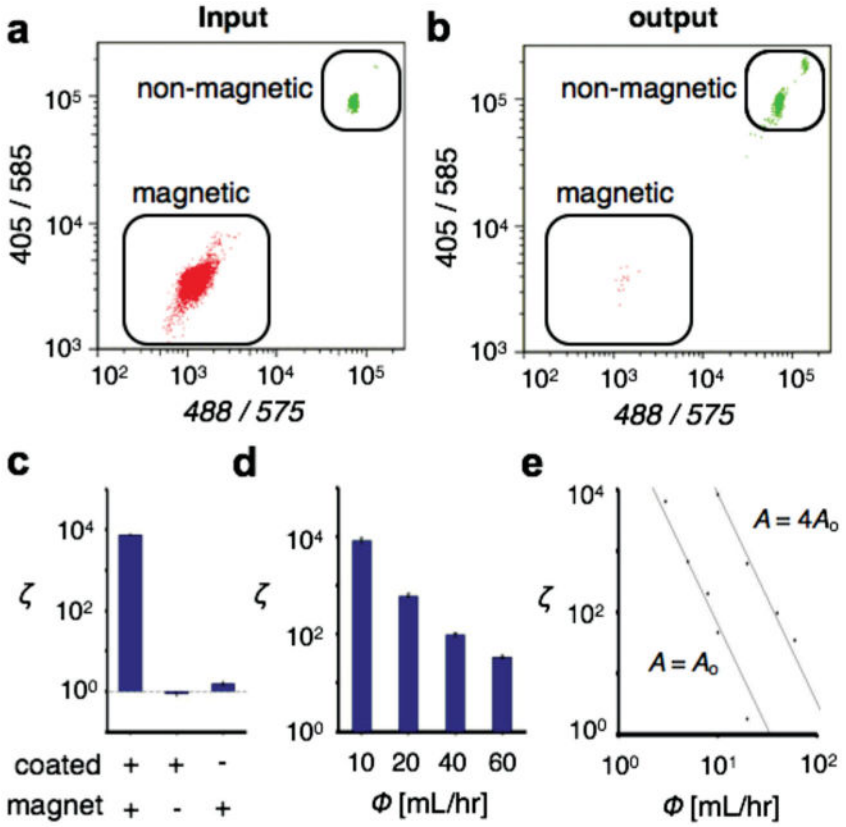

Figure 3.

Characterization of the TEMPO filter. The TEMPO filter was tested by filtering a population of magnetic from non-magnetic polystyrene beads. Flow cytometry quantified the bead population a) before and b) after the filtration. c) Comparison of enrichment with (+) and without (−) the permalloy coating on the TEMPO and the external magnet. The enhancement due to the permalloy coating was 5000×. d) The TEMPO filter achieved a very high enrichment ζ, enhancing the population of polystyrene beads to magnetic ones by a factor of $\zeta > 10^4$, at flow rates $\boldsymbol{\Phi} > 10$ mL h^{-1}. The enrichment ratio ζ was measured for flow rates up to 60 mL h^{-1}. e) The enrichment ζ was shown to depend on flow rate $\boldsymbol{\Phi}$ as a power law. An increase in the area *A* of the TEMPO, shifted the enrichment ζ vs flow-rate linearly, but did not change the power-law dependence.

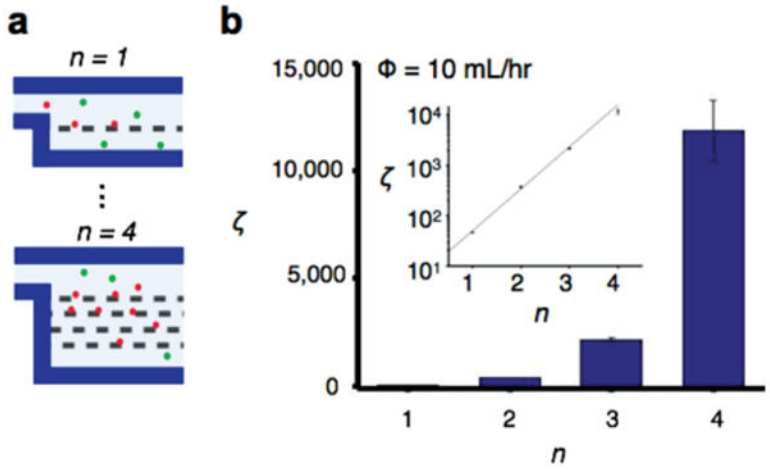

Figure 4.

Serial enrichment with TEMPO filters. a) The TEMPO filters can be integrated in series on a microfluidic chip, with the output of each TEMPO becoming the input of the subsequent filter. b) A large enhancement (250×) in enrichment ζ was observed going from $n = 1$ to $n = 4$ filters. In the inset enrichment ζ vs number of filters, n is plotted on a semi-log plot and is fit with an exponential increase.

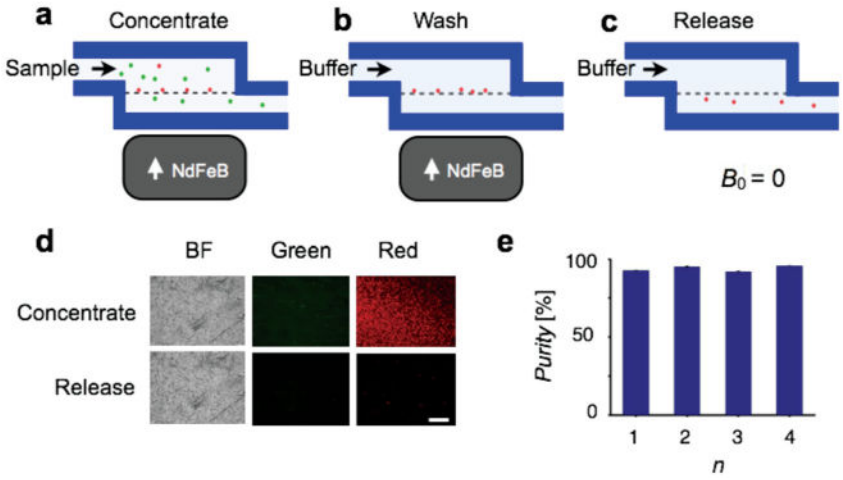

Figure 5.

Trap and release with the TEMPO. When the external NdFeB magnet is removed, the magnetic force disappears and the trapped cells can be released from the TEMPO. To trap and release cells, targeted cells are a) first trapped by passing the sample through the TEMPO filter with the external magnet in place, b) the trapped are washed by passing buffer solution, and c) the external magnet is removed and the trapped cells are released. d) Fluorescence image of cells on the TEMPO in bright field (BF) and green and red fluorescence channels during isolation of the cells and after release. The scale bar is 250 μm. e) The released beads were >95% pure from contamination of green beads, and this purity did not significantly change with additional layers *n* of TEMPO

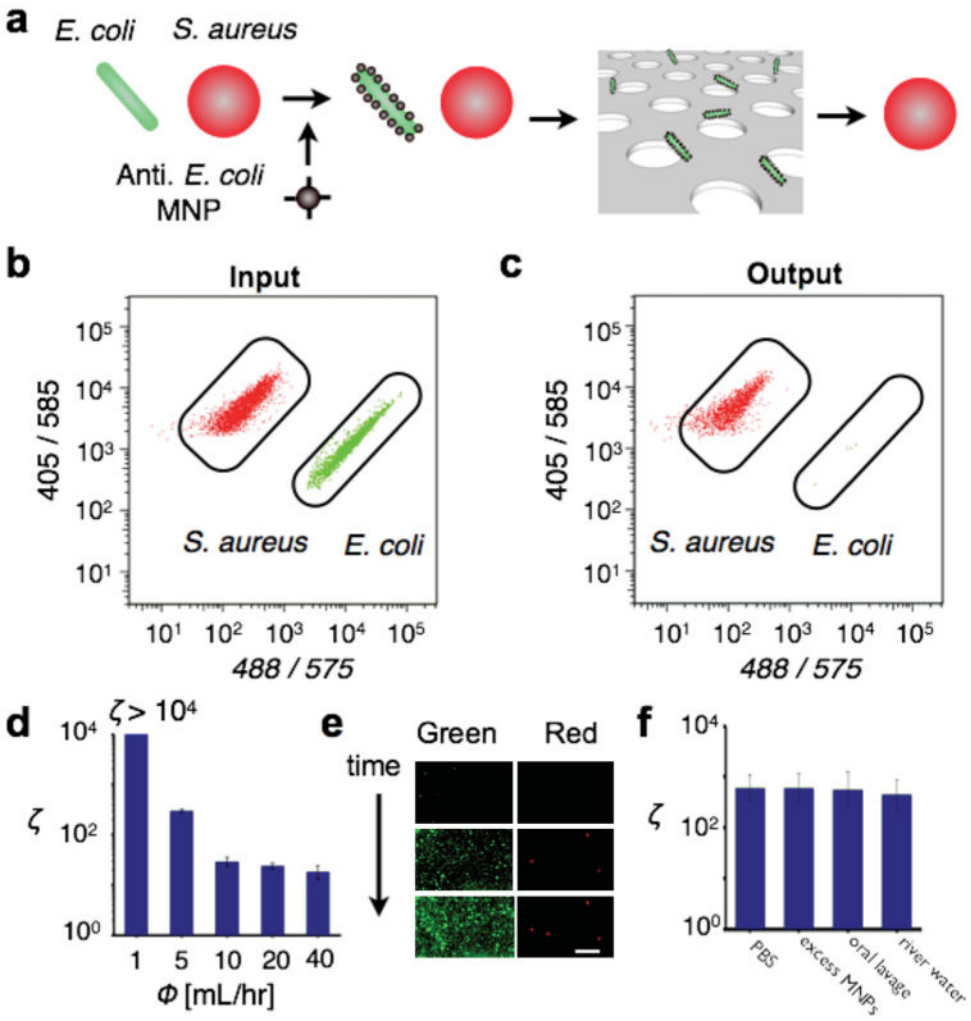

Figure 6.

Species-specific enrichment of pathogens from complex samples. a) *E. coli* (stained green) suspended among a negative control of *S. aureus* (stained red) were magnetically labeled and isolated using the TEMPO filter. b) Flow cytometry was used to quantify the cell population before b and after c the filtration, demonstrating that the *E. coli* could be efficiently isolated from the suspension. d) The TEMPO filter achieves a very high enrichment ζ, enhancing the population of *E. coli* to *S. aureus* by a factor of ζ = 600 at $\boldsymbol{\Phi} = 5$ mL h^{-1}. The enrichment ratio ζ was measured for flow rates up to 40 mL h^{-1}. e) Fluorescence images were taken of the bacteria in real-time as they are trapped onto the TEMPO. The initial population of *S. aureus* was 20× that of *E. coli*. The enriched population of *E. coli* (green) can be counted with little contamination from the background population of *S. aureus* (red). The scale bar is 20 μm. f) The TEMPO was insensitive to the background of unprocessed clinical and environmental samples. The magnetically labeled bacteria were enriched from spiked samples, including PBS, PBS + excess MNPs, oral lavage from a healthy volunteer, and water collected from a local river.